Cluster mean-field study of the Heisenberg model for $CuInVO_5$

Ayushi Singhania and Sanjeev Kumar
Indian Institute of Science Education and Research Mohali, Sector 81, S.A.S. Nagar, Manauli PO 140306, India

(Received 3 May 2018; revised manuscript received 5 August 2018; published 26 September 2018)

Motivated by the experimental report of unusual low-temperature magnetism in the quasi-one-dimensional magnet $CuInVO_5$, we present results of a cluster mean-field study on a spin-1/2 Heisenberg model with alternating ferromagnetic and antiferromagnetic nearest-neighbor coupling. We map out the ground-state phase diagrams with varying model parameters, including the effect of an external magnetic field. An unexpected competition between different spin-spin correlations is uncovered. Multiple spin-flop transitions are identified with the help of component-resolved correlation functions. For the material-specific choice of model parameters we discuss the temperature dependence of specific heat and magnetic susceptibility and compare our results with the available experimental data. A detailed account of spin-spin correlations allows us to present a microscopic understanding of the low-temperature magnetic ordering in $CuInVO_5$. Most notably, we identify the origin of an extra peak in the low-temperature specific heat data of $CuInVO_5$ reported by Hase *et al.* [Phys. Rev. B **94**, 174421 (2016)].

DOI: 10.1103/PhysRevB.98.104429

I. INTRODUCTION

Spin-1/2 quasi-one-dimensional (Q1D) magnets are ideal candidates for observing fundamental quantum phenomena as the combination of low dimensionality and small spin magnitude maximizes quantum fluctuations [1,2]. This has motivated experimentalists for many decades to realize one-dimensional quantum magnets [3,4]. These efforts have led to the discovery of many Q1D magnets and to the experimental verification of various quantum phenomena [5]. Indeed, quantum phase transitions driven by magnetic field or external pressure have been reported in low-dimensional magnets such as $TlCuCl_3$, $KCuCl_3$, $LiCuVO_4$, $CoNb_2O_6$, etc. [6–13]. Certain low-dimensional magnets have also been identified as being close to a quantum critical point [14,15]. The presence of the extended quantum critical region has been inferred from the magnetic field dependence of excitations in copper pyrazine dinitrate [16]. Due to enhanced quantum fluctuations, Q1D magnets are also considered strong candidates for hosting quantum spin liquid states [10,17–19]. Another aspect that makes low-dimensional magnets very interesting is the possibility of a qualitatively new type of excitations [20–22]. A classic example is that of spinon excitations in one-dimensional antiferromagnets [23,24]. More recently, the realization of longitudinal spin excitations, the so-called Higgs mode, in certain Q1D magnets was proposed [25–31].

Recent experimental studies on the spin-1/2 tetramer compound $CuInVO_5$ show unusual magnetism at low temperatures [25]. Thermodynamic measurements, such as specific heat and magnetic susceptibility, show that a long-range ordered antiferromagnetic state exists below 2.7 K. There are two inequivalent Cu sites, and the size of the ordered moment strongly differs at these two sites. This leads to a magnetization plateau in the magnetic field dependence at nearly half the saturation magnetization. While some of the features observed in $CuInVO_5$ can be explained within a simple mean-field approach, the presence of two peaks in the low-temperature specific heat and the presence of a cusp in the magnetic susceptibility remain two of the unexplained features in the data [25]. Furthermore, a microscopic picture of the ordered state and its evolution with magnetic field and temperature has been lacking.

Motivated by these puzzles in the experimental data on $CuInVO_5$, we present a comprehensive analysis of a four-sublattice one-dimensional Heisenberg model with three different nearest-neighbor exchange couplings. We make use of the cluster mean-field (CMF) approach in which intracluster interactions are treated exactly while intercluster interactions are treated at the mean-field level. The approach is well justified in the context of $CuInVO_5$ due to the existence of a hierarchy of coupling strengths as inferred from the experimental results [25]. We find that treating intertetramer coupling beyond mean field, which requires a minimum of eight sites in the cluster for the CMF study, brings out a subtle competition between two different spin-spin correlations. This emphasizes the presence of two distinct limiting phases in the model, and the ground state in $CuInVO_5$ is best understood as a compromise of these two competing tendencies. Interestingly, the temperature dependence of the correlations is nonmonotonic with certain spin-spin correlations strengthening with increasing temperature. Such effects are typically encountered in frustrated magnets where entropic effects at higher temperatures can help in the enhancement of the order [32–34]. We also identify multiple spin-flop transitions in the presence of external field which highlight the inequivalence of spins within a tetramer. Most importantly, the subtle interplay between different spin-spin correlations accounts for the presence of an extra peak in the magnetic specific heat and a cusp in the magnetic susceptibility at low temperatures, in excellent agreement with the experimental data on $CuInVO_5$ [25].

The remainder of the paper is organized as follows. In Sec. II we define the model and discuss the CMF approach used for the study. Results are discussed in Sec. III, where we begin by discussing the phase diagrams for the general choice of model parameters. This is followed by a discussion of various observables calculated for the parameters specific to $CuInVO_5$. For a clear understanding of the microscopic details we analyze the longitudinal and transverse spin-spin correlations between different pairs of spins. A summary and conclusions are presented in Sec. IV.

II. MODEL AND METHOD

We begin with a Heisenberg model on a 1D chain of spin-1/2 tetramers in the presence of an external magnetic field. The model is described by the Hamiltonian

$$H = \sum_{i=1}^{N_t}[J_2(\mathbf{S}_{4i-3}\cdot\mathbf{S}_{4i-2}+\mathbf{S}_{4i-1}\cdot\mathbf{S}_{4i})+J_1\mathbf{S}_{4i-2}\cdot\mathbf{S}_{4i-1} + J_3\mathbf{S}_{4i}\cdot\mathbf{S}_{4i+1}] - h_z\sum_{i=1}^{N_t}\sum_{j=0}^{3}S^z_{4i-j}. \quad (1)$$

Here, $\mathbf{S}_{4i-j}$, with $j = 0, 1, 2, 3$, are the Heisenberg spin operators belonging to the ith tetramer. $J_1 > 0$, $J_2 < 0$, $J_3 > 0$ are the Heisenberg exchange constants, and h_z is the magnitude of the applied magnetic field. N_t is the total number of tetramers, and the periodic boundary condition is imposed via the identification $\mathbf{S}_{4N_t+1} \equiv \mathbf{S}_1$. For the analysis of the model Hamiltonian we will use $J_1 = 1$ as the elementary energy scale. This leaves us with J_2, J_3, and h_z as free model parameters. The intertetramer exchange J_3 is inferred to be much smaller than the intratetramer couplings J_1 and J_2 in $CuInVO_5$.

In order to understand the nature of long-range magnetic order in the model Hamiltonian Eq. (1), we employ the CMF approach. The CMF method is an extension of the single-site Weiss mean-field approximation and has been very successful in studying the competition between different ordered states even in low dimensions [35–37]. It is well known that the Mermin-Wagner theorem prohibits the presence of any long-range order at nonzero temperatures for isotropic spin Hamiltonians in dimensions $d \leqslant 2$ [38]. However, most low-dimensional magnets exhibit long-range order at small but finite temperatures [4,39,40]. $CuInVO_5$ is no exception to this trend as a long-range order sets in at 2.7 K. This apparent violation of Mermin-Wagner theorem can be understood in terms of the presence of magnetic anisotropies and/or the role of weaker interchain or interlayer coupling. The importance of quantum effects in low-dimensional ordered magnets is typically reflected in the suppression of the ordered moment [41]. The existence of long-range magnetic order in $CuInVO_5$ further justifies the use of the CMF approach for describing low-temperature magnetism. One can argue that the mean-field aspect of the method takes into account the three-dimensional character of the magnetic system. Hence, the feature that CMF calculations lead to an ordered state at low enough temperatures is consistent with the experimental results.

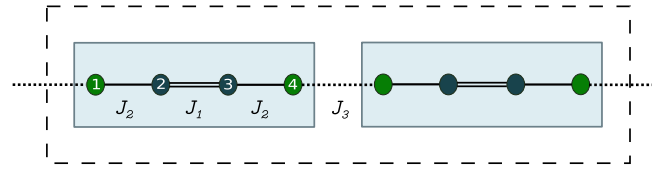

FIG. 1. Schematic picture of the coupled tetramer model. Each dot represents a spin-1/2, and the nearest-neighbor couplings are indicated by double (J_1), solid (J_2), and dotted (J_3) lines.

Although the CMF approach has been extensively discussed in the literature [36,37], for completeness, we briefly introduce the method here. Specifically, let us consider a one-dimensional system which can be thought of as a repeated structure of clusters containing linear segments of N_c spins. We want to treat the interactions within the cluster exactly, while intercluster interactions will be treated approximately. In a one-dimensional system there are two edge spins, $\mathbf{S}_1$ and $\mathbf{S}_{N_c}$, that couple the central cluster to two adjacent clusters (see Fig 1). These two intercluster coupling terms can be approximated via the standard mean-field decoupling where $\mathbf{S}_i\cdot\mathbf{S}_{i+1}$ is replaced by $\langle\mathbf{S}_i\rangle\cdot\mathbf{S}_{i+1}+\mathbf{S}_i\cdot\langle\mathbf{S}_{i+1}\rangle-\langle\mathbf{S}_i\rangle\cdot\langle\mathbf{S}_{i+1}\rangle$ by ignoring the higher-order fluctuation terms. Therefore, the original Hamiltonian reduces to a cluster Hamiltonian in the presence of mean fields that are experienced by the edge spins. The mean fields acting on spins $\mathbf{S}_1$ and $\mathbf{S}_{N_c}$ are then calculated self-consistently. For a cluster with N_c spins of magnitude 1/2, the size of the Hilbert space for the cluster Hamiltonian is 2^{N_c}, and therefore, the cluster Hamiltonian can be easily diagonalized exactly for $N_c \leqslant 12$. Note that in the general case where the mean fields are allowed to have components along the x and y directions, the resulting mean-field Hamiltonian does not possess many of the symmetries of the full interacting Hamiltonian. Therefore, it is not generally possible to make use of symmetries to achieve diagonalizations of larger clusters. The quantum expectation values of the spin operators $\langle S^\alpha_i\rangle$, where i denotes the site and α denotes the spin component, can be computed following the standard quantum-statistical mechanics. The angular brackets denote the quantum-statistical average of the operator and are defined for any operator O as

$$\langle O\rangle = \frac{1}{\mathcal{Z}}\mathrm{Tr}\,[O\,e^{-\beta H_c}], \quad (2)$$

where β is the inverse temperature, H_c is the cluster Hamiltonian, and $\mathcal{Z} = \mathrm{Tr}\,e^{-\beta H_c}$ is the partition function. The process is repeated until a self-consistent solution is obtained up to a desired tolerance factor. In our calculations we take 10^{-5} as the tolerance factor for convergence. As with all self-consistent approaches, we begin with a variety of initial mean-field configurations to ensure that the resulting self-consistent solution corresponds to a global minimum.

III. RESULTS AND DISCUSSION

Before we consider the model parameters relevant to $CuInVO_5$, it is useful to explore the ground-state phase diagrams of the model in the parameter space $|J_2|/J_1$, J_3/J_1, and h_z/J_1. To obtain these CMF phase diagrams we work with an eight-site cluster containing two tetramers. The justification

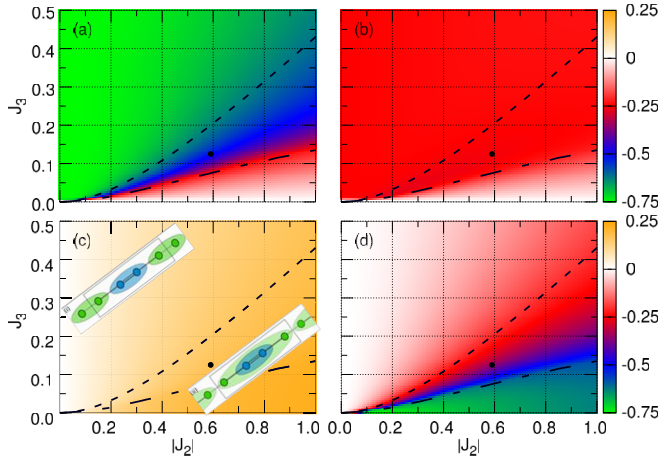

FIG. 2. Variation of different spin-spin correlations with $|J_2|/J_1$ and J_3/J_1 for $h_z = 0$: (a) C_{45}, (b) C_{18}, (c) C_{12}, and (d) C_{14}. C_{ij} are computed within the CMF approach using an eight-site cluster. The dot indicates the location of the magnetic model for $CuInVO_5$ in the $|J_2|$-J_3 plane. The dashed line is an estimate for the path in parameter space where two different tendencies for singlet formation strongly compete (see the text). In (c) we show the schematic picture of two limiting states. The long- and short-dashed line marks the separation between the Néel-type long-range ordered state and the state consisting of noninteracting tetramers.

for this choice will become clear in Secs. III B and III C, where we will present a comparison between results obtained using four-site and eight-site clusters.

A. Spin-spin correlations in the ground state

In order to characterize the ordered states at low temperature, we compute the transverse and longitudinal components of the spin-spin correlations defined as

$$C_{ij}^{\perp} = \tfrac{1}{2}\langle S_i^+ S_j^- + S_i^- S_j^+\rangle, \quad C_{ij}^{zz} = \langle S_i^z S_j^z\rangle. \tag{3}$$

The total spin-spin correlations C_{ij} can be obtained by adding the transverse and longitudinal components, $C_{ij} = C_{ij}^{\perp} + C_{ij}^{zz}$.

In the absence of external magnetic field, we present the evolution of total spin-spin correlations as a function of $|J_2|$ and J_3, keeping $J_1 = 1$ as the strongest exchange parameter. As expected, we find that C_{23} retains its singlet-like character across the entire parameter regime covered in Fig. 2 [42]. Similarly, C_{12} and C_{34} [see Fig. 2(c)] remain ferromagnetic in nature, except in the vicinity of the $J_2 = 0$ line, where these correlations become vanishingly small. The behavior of C_{23} (C_{12}/C_{34}) is not at all surprising since these spins are directly coupled via antiferromagnetic (ferromagnetic) interactions. A most interesting variation is noticed in C_{14} and C_{45}. C_{45} begins with a perfect singlet nature ($C_{45} \approx -0.75$) along the $J_2 = 0$ line, and the correlations diminish gradually as we move towards the $J_3 = 0$ line. The behavior of C_{14} is complementary to that of C_{45}. This can be easily understood as $\mathbf{S}_4$ being able to participate in only one perfect singlet, either with $\mathbf{S}_1$ or with $\mathbf{S}_5$. The tendency for singlet formation between $\mathbf{S}_4$ and $\mathbf{S}_5$ is easy to understand as these two spins are directly coupled via J_3. On the other hand, the singlet between $\mathbf{S}_1$ and $\mathbf{S}_4$ is mediated via an antiferromagnetic exchange J_1 and a ferromagnetic exchange J_2. The perfect singlet character for either pair is disturbed when all the interaction strengths are finite. Instead, a compromise state with antiferromagnetic (AFM) correlations between both the $\mathbf{S}_1$-$\mathbf{S}_4$ and $\mathbf{S}_4$-$\mathbf{S}_5$ pairs is preferred. It is important to note that this subtle competition is not captured in calculations that limit the cluster size to four sites (single tetramer), as in that case C_{45} cannot be distinguished from C_{14}. The correlation C_{18} originates from the intercluster couplings where $\mathbf{S}_1$ and $\mathbf{S}_8$ belonging to the central cluster are coupled to mean fields of $\mathbf{S}_8$ and $\mathbf{S}_1$, respectively. As expected, we find that this mean-field treatment restricts the correlation strengths to the classical value of -0.25 [see Fig. 2(b)].

The behavior of correlations between different spin pairs in the cluster points to the following three distinct ground states: (i) The simplest limit corresponds to $J_3 \to 0$ and $J_2 \to 0$, where the system is a collection of $\mathbf{S}_2$-$\mathbf{S}_3$ singlets and isolated spins $\mathbf{S}_1$ and $\mathbf{S}_4$. (ii) If J_3 dominates over J_2, then the system can be considered to be close to a valance bond solid limit where two different types of singlets, one due to J_1 coupling and the other due to J_3 coupling, are formed [see the schematic picture in the top left corner in Fig. 2(c)]. Of course, the exact singlet correlations are spoiled by the presence of the ferromagnetic J_2 coupling and also by the CMF treatment. As a consequence, an $\uparrow\uparrow\downarrow\downarrow$-type antiferromagnetic ordering with reduced magnetic moments emerges. (iii) Finally, in the case of $|J_2|$ dominating over J_3, the C_{14} correlation achieve values close to that of a perfect singlet, i.e., -0.75, while C_{45} is almost uncorrelated [compare Figs. 2(a) and 2(d) and see the schematic picture in the bottom right corner in Fig. 2(c)]. By plotting the change in the self-consistent mean fields $\langle S_1^z\rangle$ and $\langle S_8^z\rangle$ as a function of $|J_2|$ for fixed values of J_3 [43], we identify this limit in terms of the inequality $|J_2| > 8J_3$, marked by a long- and short-dashed line in Fig. 2. The ground state in the region $|J_2| > 8J_3$ corresponds to that of an isolated four-site cluster. The magnetic phase diagram as inferred from C_{ij} therefore consists of the three qualitatively distinct regimes discussed above, which are connected to each other continuously.

It is instructive to quantify the competition between different limiting cases. Figures 2(a) and 2(d) suggest that the key competition is between the singlet correlations C_{14} and C_{45}. Solving the isolated eight-site cluster with open boundary conditions, we find that the ground-state energy is given by

$$E_1 = -\tfrac{1}{4}\big(J_1 + 2J_2 + 2\sqrt{J_1^2 - 2J_1J_2 + 4J_2^2}\big). \tag{4}$$

On the other hand, the state in the limit $J_2 = 0$ is a collection of alternating singlets with energy per tetramer

$$E_2 = -\tfrac{3}{4}(J_1 + J_3). \tag{5}$$

Therefore, the competition between these two tendencies is strongest when the two energy contributions are equal. This gives us a relation between J_2 and J_3 which is obtained by numerically solving Eqs. (4) and (5). The result is plotted as a dashed line in Figs. 2(a) and 2(d). The dots in Fig. 2 represent the location of the magnetic model for $CuInVO_5$ in the parameter space of the model (1). We note that $CuInVO_5$ is not far from this strongly competing regime; therefore,

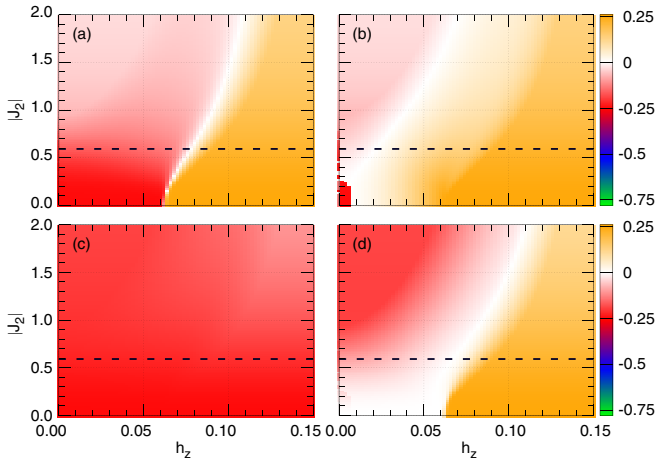

FIG. 3. Variation of the longitudinal component of spin-spin correlations with $|J_2|/J_1$ and h_z/J_1 for $J_3/J_1 = 0.125$: (a) C^{zz}_{45}, (b) C^{zz}_{18}, (c) C^{zz}_{23}, and (d) C^{zz}_{14}. Dashed horizontal lines correspond to the $|J_2|/J_1$ ratio estimated for $CuInVO_5$.

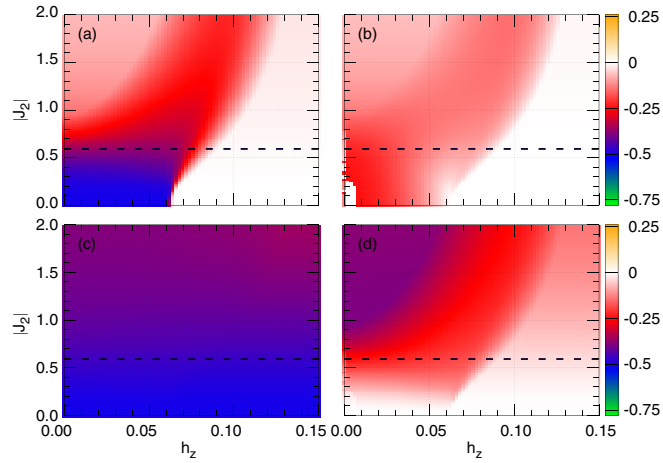

FIG. 4. Variation of the transverse component of spin-spin correlations with $|J_2|/J_1$ and h_z/J_1 for $J_3/J_1 = 0.125$: (a) $C^{\perp}_{45}$, (b) $C^{\perp}_{18}$, (c) $C^{\perp}_{23}$, and (d) $C^{\perp}_{14}$. Dashed horizontal lines correspond to the $|J_2|/J_1$ ratio estimated for $CuInVO_5$.

treating the C_{45} correlations exactly is very important to capture the important aspects of magnetism in $CuInVO_5$.

Next, we look at the dependence of spin-spin correlations on external magnetic field. In this case we discuss both the longitudinal and transverse components of the correlations. For this purpose we fix the value of the intertetramer exchange $J_3 = 0.125$ and explore the phases in the h_z-J_2 plane. The specific choice of the J_3 value is relevant to $CuInVO_5$, where J_1 and J_3 are estimated to be 240 and 30 K, respectively [25]. For small values of J_2, the longitudinal and transverse components of C_{23} are close to -0.25 and -0.50, respectively. These singletlike correlations for C_{23} remain unaffected by the external magnetic field in the regime $|J_2| < 1$. Interesting conclusions can be drawn by comparing the field dependence of component-resolved C_{18} and C_{45}. For small J_2, C_{18} starts off with AFM correlations in the z component and no correlations in the transverse direction, i.e., $C^{zz}_{18} = -0.25$ and $C^{\perp}_{18} = 0$ [see Figs. 3(c) and 4(c)]. A sharp change in these correlations is found near $h_z = 0.01$, where the longitudinal component becomes close to zero and the transverse component increases to -0.25. This is a clear signature of the spin-flop state involving a flopping of $\mathbf{S}_1$ and $\mathbf{S}_8$. The longitudinal component then gradually increases to positive values at the cost of a reduction in transverse correlations, in accordance with the standard picture of a spin-flop state evolving towards a canted state. Following the change in components of C_{45} (say, at $J_2 = -0.58$, which is relevant for $CuInVO_5$) upon varying magnetic field highlights a similar effect for the $\mathbf{S}_4$-$\mathbf{S}_5$ pair. The transverse correlations decrease sharply near $h_z = 0.08$, and the longitudinal correlations vanish and then rapidly rise to positive values. Thus, a clear picture emerges for the presence of two spin-flop transitions in this spin-1/2 tetramer model: the first one corresponding to a flopping of edge spins and the second one corresponding to that of the central pair of spins. For still larger values of h_z, another spin-flop corresponding to the $\mathbf{S}_2$-$\mathbf{S}_3$ pair is present. Note that the anticorrelation between C_{14} and C_{45} is also present for finite magnetic fields [see Figs. 3(a), 3(d), 4(a), and 4(d)].

Having discussed the broad picture for different spin-spin correlations and their component-resolved evolution with magnetic field, we now focus on the parameter values considered relevant for $CuInVO_5$. We begin by discussing results for a four-site cluster.

B. Single-tetramer cluster

In this section, we discuss results obtained via the CMF approach using a four-site cluster. We begin by comparing the temperature dependence of spin-spin correlations obtained for an isolated tetramer and those from CMF with a four-site cluster. In the case of an isolated tetramer, the cluster is treated exactly with open boundary conditions where, as in the case of CMF, edge spins $\mathbf{S}_1$ and $\mathbf{S}_4$ couple to average fields $\langle \mathbf{S}_4 \rangle$ and $\langle \mathbf{S}_1 \rangle$, respectively, via J_3. The difference in the two sets of correlation functions vanishes above $\sim$8 K. This indicates that the self-consistent mean fields vanish above 8 K, and the long-range order, which can be captured via the CMF approach, is present below 8 K. Indeed, the main advantage of using a mean-field approach is to obtain results in the thermodynamic limit. However, we point out a crucial shortcoming of the CMF approach applied to this system. The correlation C_{14} for the two edge spins of a tetramer are treated better in an isolated tetramer. These correlations have a value, $C_{14} \approx -0.68$, close to that of a perfect singlet. In the mean-field approach the edge spins are coupled to average fields due to finite $\langle \mathbf{S}_1 \rangle$ and $\langle \mathbf{S}_4 \rangle$, and therefore, the correlations are strongly reduced. This can be observed for all the correlations involving the edge spins (see Fig. 5). The correlation of the central spin pair C_{23} is identical in the two calculations, as expected.

In addition to computing spin-spin correlation functions defined in Eq. (3), we also compute quantities that can be compared directly with the experiments. To this end, we compute the specific heat and the magnetic susceptibility using the standard definitions

$$C_V(T) = \frac{d\langle H \rangle}{dT}, \quad \chi(T) = \frac{d\langle M_z \rangle}{dh_z}. \tag{6}$$

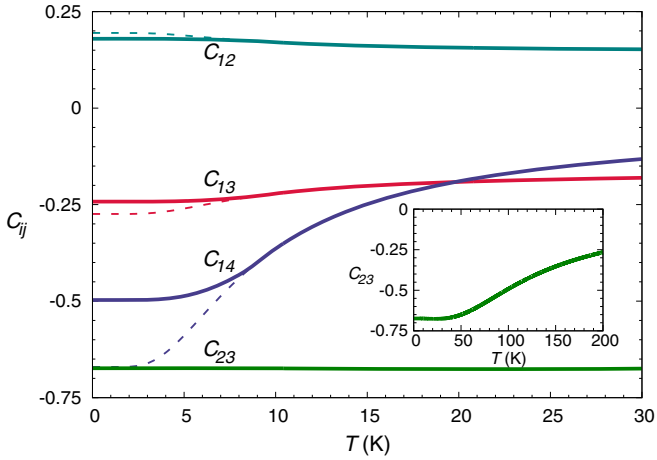

FIG. 5. Spin-spin correlations C_{ij} as a function of temperature for an isolated tetramer (dashed lines) and within the CMF approach using a four-site cluster (solid lines). Variation of C_{23} over a larger T scale is shown in the inset.

We now present the comparison of specific heat calculations for an isolated cluster and for the four-site CMF approximation. For an isolated cluster the ground state belongs to the $S_T = 0$ sector and is characterized by singlet correlations between spin pairs $\mathbf{S}_1$-$\mathbf{S}_4$ and $\mathbf{S}_2$-$\mathbf{S}_3$. This is, indeed, reflected in Fig. 5, where the pair correlations C_{23} and C_{14} are found to be close to a perfect singlet type. Treating the intertetramer interactions at the mean-field level spoils the singlet correlation C_{14} as the edge spins now experience classical mean fields. The specific heat for an isolated cluster (Fig. 6) shows two broad peaks which can be naively associated with the loss of correlations C_{14} at around 10 K and the breaking of the stronger singlet between the central Cu spins at around 100 K. The CMF results lead to a sharp peak in C_V, signifying the onset of long-range order below ∼8 K.

In order to confirm the simple picture proposed from the spin-spin correlation and the specific heat calculations, we now show the magnetic susceptibility results. If the simple picture of a two-step loss of correlations is indeed true, then it should have specific consequences for the behavior of

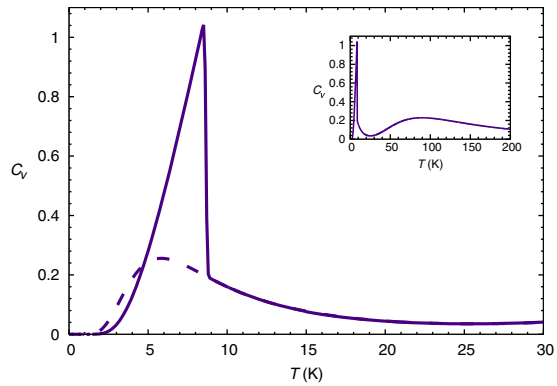

FIG. 6. Specific heat as a function of temperature for an isolated tetramer (dashed line) and for the CMF approximation with a four-site cluster (solid line). The inset shows the behavior over a wider temperature scale for the CMF approximation.

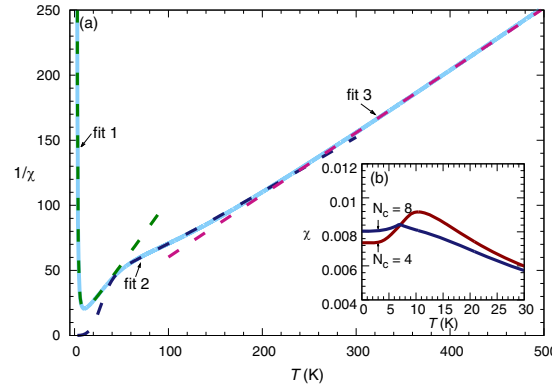

FIG. 7. (a) Inverse magnetic susceptibility χ^{-1} as a function of temperature for an isolated tetramer. The dashed lines are the best fits corresponding to three different temperature regimes (see text). (b) The result for $\chi(T)$ within the CMF approximation using four-site and eight-site clusters.

magnetic susceptibility. To verify this, we plot the inverse magnetic susceptibility obtained for an isolated cluster in Fig. 7(a). Given the tendency for singlet formation at low temperatures, we fit the magnetic susceptibility differently in three temperature regimes. In the range 0 K $< T <$ 40 K, we fit the susceptibility via the following behavior for singlets [44,45]:

$$\chi(T) = \frac{a_1}{T}\frac{e^{(-b_1/T)}}{1+3e^{(-b_1/T)}}. \tag{7}$$

In the above, the fitting parameter a_1 contains information about the number of singlets, and b_1 is related to the excitation gap. In the regime 40 K $< T <$ 300 K, the system should display a mixed behavior since the weaker singlets cease to exist and the participating spins will now contribute as free paramagnetic moments. Therefore, we fit the susceptibility via

$$\chi(T) = \frac{a_2}{T}\frac{e^{(-b_2/T)}}{1+3e^{(-b_2/T)}} + \frac{c_2}{T-d_2}. \tag{8}$$

The second term is simply the Curie-Weiss behavior, and the two fitting parameters contain information regarding the total number of paramagnetic moments and the Curie-Weiss temperature. In the high-temperature regime, one expects a total Curie-Weiss behavior for all the constituent spins. Therefore, a Curie-Weiss fit, $\chi(T) = \frac{c_3}{T-d_3}$, is used in the range 300 K $< T <$ 600 K. The actual $\chi^{-1}(T)$ and the three fits discussed above are shown in Fig. 7(a). From the quality of the fit the following simple picture is reconfirmed. At low temperature, the magnetic susceptibility fits very well to a singlet behavior. At intermediate temperatures, two of the spins get free and contribute to the Curie-Weiss susceptibility. Finally, a paramagnetic behavior emerges at high temperatures. The obtained fit parameters differ slightly from the above picture in terms of the number of spins contributing to susceptibility as singlets or paramagnetic moments at different temperatures [45].

We find that while the tendency for singlet formation below 100 K between $\mathbf{S}_2$ and $\mathbf{S}_3$ and the long-range order to a Néel state with the ↑↑↓↓ pattern below about 10 K is obtained within the four-site CMF approach, the experimental

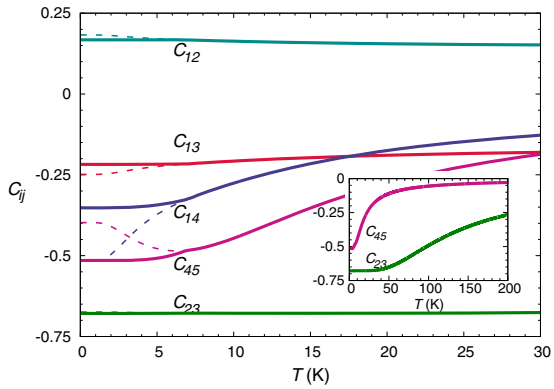

FIG. 8. Spin-spin correlations C_{ij} as a function of temperature for an isolated eight-site cluster (dashed lines) and within the CMF approach using an eight-site cluster (solid lines). Variations in C_{23} and C_{45} over a wider T range are shown in the inset.

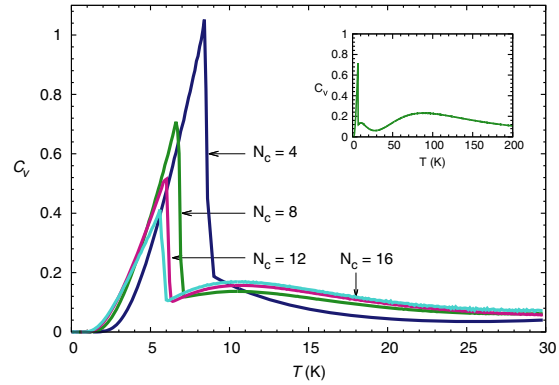

FIG. 9. Specific heat as a function of temperature within the CMF approximation for 4-site, 8-site, 12-site, and 16-site clusters. The behavior across a broader temperature scale is displayed in the inset.

observation of a second peak in the specific heat at about 2.7 K is not consistent with the CMF results. We argue that treating intertetramer interactions beyond mean field is the key to understanding the magnetism of $CuInVO_5$. We discuss the eight-site CMF results in the next section. Nevertheless, we already find that eight-site CMF results for magnetic susceptibility are qualitatively different from those obtained for four-site CMF [see Fig. 7(b)]. A cusplike feature followed by a broad hump is reported in the experiments which seems to be captured within eight-site CMF calculations. Clearly, if the interaction J_3 happens to be stronger than the ferromagnetic interaction J_2, then the system would prefer to form singlets between $\mathbf{S}_2$ and $\mathbf{S}_3$ and $\mathbf{S}_4$ and $\mathbf{S}_5$ instead of a pair of singlets within a tetramer. In fact, even if J_3 is much smaller than J_2, since J_3 is antiferromagnetic in nature, it may be important to retain the correlations in the intertetramer interaction. The simplest way to achieve this is to increase the cluster size to eight spins (two-tetramers) for which one central intertetramer exchange term will be treated exactly. Next, we present the results for CMF using two- and three-tetramer units as the cluster.

C. Beyond a single-tetramer cluster

We begin by presenting the spin-spin correlation functions for different pairs as a function of temperature. Note that the most important correlation that was missing in the four-site cluster treatment is C_{45}. The exact solution of the isolated eight-site cluster shows that at $T = 0$, C_{14} is antiferromagnetic in nature and larger in magnitude than C_{45}. With increasing temperature $|C_{14}|$ reduces rapidly (see Fig. 8). Interestingly, this decrease of $|C_{14}|$ is accompanied by an increase of $|C_{45}|$. Note that it is rather unusual to find an increase in the magnitude of correlations as a function of temperature. This hints at competing tendencies for order in the ground state. We can comprehend this finding as follows. Spin $\mathbf{S}_4$ can have singlet-type correlations with $\mathbf{S}_5$ due to the antiferromagnetic exchange constant J_3. However, it can also have quantum antiferromagnetic correlations with spin $\mathbf{S}_1$ due to the combined effect of an antiferromagnetic J_1 and ferromagnetic J_2. These two tendencies for singlet correlations are competing in the ground state, and for the material-specific values of the exchange parameters a dominant antiferromagnetic correlation with spin $\mathbf{S}_1$ is energetically favored. With increasing temperature, a weakening of longer-range correlations (C_{14}) allows for strengthening of C_{45}. This intriguing interplay of two competing tendencies for singlet formation is apparent in our discussion of the model for generic parameter values [compare Figs. 2(a) and 2(d)]. Interestingly, this competition between different singlet choices is also at play when temperature varies and has consequences for physical observables. The fact that different spin-spin correlations are being affected at different temperatures should be reflected in specific heat results. To verify this we plot in Fig. 9 the specific heat calculated within the CMF approach using 4-, 8-, 12-, and 16-site clusters [46]. In contrast to the results for a 4-site cluster, two peaks at low temperatures are found in the 8-, 12-, and 16-site CMF calculations.

The results suggest that the most important improvement to the four-site CMF results already occurs when we use an eight-site cluster and hence treat intertetramer interaction exactly. The relative strength and position of the two low-temperature peaks in C_V change as we increase the cluster size (see Fig. 10). The first peak which is related to the long-range order reduces with increasing system size. Although the scaling based on three data points is not conclusive, the estimates for the peak locations T_p obtained from the extrapolated data are in very good agreement with the experiments with an

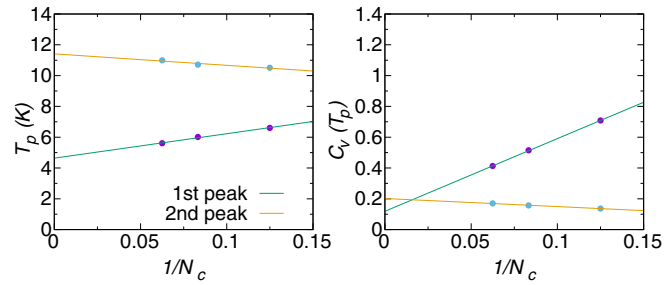

FIG. 10. Scaling of peak locations T_p and peak values $C_V(T_p)$ in the specific heat shown in Fig. 9 with inverse cluster size.

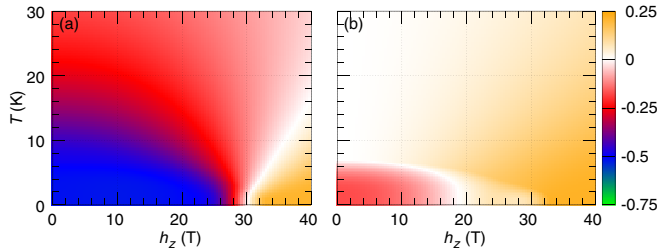

FIG. 11. Temperature and field dependence of (a) spin-spin correlations C_{45} and (b) the product of mean-field variables $\langle \mathbf{S}_1 \rangle \cdot \langle \mathbf{S}_8 \rangle$ for the parameter values specific to $CuInVO_5$. The temperature (magnetic field) axis is in kelvins (teslas). Note that the quantity plotted in (b) is finite for a long-range ordered magnetic state.

overestimation of about 1.5 K. More importantly, it is ruled out that any new peaks in the specific heat arise with adding more tetramers to the cluster used in the CMF approach. Note that the experimental plot for C_V also contains a contribution from phonons which needs to be subtracted in order to identify the pure magnetic contribution. While the phonon contribution will mask the high-temperature peak around 90 K (see the inset in Fig. 9), the two lower-temperature peaks are easily identified in the experimental data [25].

The magnetic field dependence of the spin-spin correlations was already discussed in Figs. 3 and 4 for a generic choice of model parameters. In order to obtain the results specific to $CuInVO_5$ we simply need to find the appropriate values of model parameters. These results were obtained for $J_3/J_1 = 0.125$, a ratio motivated by the estimated values of J_1 and J_3 in $CuInVO_5$. In the material, $|J_2|/J_1$ is estimated to be 0.58, and we can focus on the $|J_2| = 0.58$ line to discuss the field dependence of correlations in $CuInVO_5$. A partial spin flop is present at low magnetic fields which leads to a magnetization plateau at $h_z = 0.08J_1$ which turns out to be around 30 T when appropriate conversion factors are included. This coincides very well with the presence of the plateau in the field dependence of magnetization (see Fig. 5 in [25]). If the simple picture of partial spin-flop transition is valid, then we should see a further increase in magnetization at yet higher magnetic fields. Indeed, we obtain saturation magnetization at about 145 T [47].

Combining the results on temperature and the magnetic field dependence of the mean-field parameters and spin-spin correlations, we present a h_z-T phase diagram in Fig. 11. The dot product of mean fields $\langle \mathbf{S}_1 \rangle \cdot \langle \mathbf{S}_8 \rangle$ is a measure of the long-range order in the system. As we can clearly see in Fig. 11(b), for small values of field there is a transition close to 5 K from a long-range ordered to disordered state. However, even in the disordered state there are certain short-range correlations that remain finite. The most important of these is C_{45}, which is shown in Fig. 11(a). These correlations remain finite up to larger temperatures and show a significant variation near $T = 10$ K. This variation is the underlying reason for a broad peak in the specific heat near 10 K. The evolution of mean-field variables with magnetic field shows that the edge spins gradually approach an aligned state starting with an antialigned state. The saturation alignment is achieved at about 30 T. Note that while the edge spins are aligned, the central spins still retain considerable singlet correlations, and therefore, the contribution to magnetization is from these edge spins leading to the magnetization plateau in the experimental data [25].

It is possible to further improve the mean-field description of the model by using different extensions of the CMF approach. Two such extensions are correlated CMF theory and quantum correlated CMF [48–50]. However, the most important aspect of the magnetic model for $CuInVO_5$ is already captured by our minimal description in which the intertetramer interaction is included in an exact manner. While some of the quantitative details, such as the relative magnitude of the low-temperature peaks, the exact location in temperature of the peaks, etc., are likely to change in a more accurate treatment of the model, the qualitative character is well described in our CMF approach.

IV. SUMMARY AND CONCLUSION

We have performed cluster mean-field analysis of a one-dimensional Heisenberg model with alternating signs of exchange constants. The choice of the model was motivated by the unusual low-temperature magnetism in $CuInVO_5$ [25]. We mapped out the nature of spin-spin correlations as a function of different model parameters. The results were obtained via the CMF approach with an eight-site cluster which, in contrast to the four-site cluster study [25], captures the effect of the intertetramer coupling beyond mean field. It turns out to be an essential ingredient for understanding some of the experimental observations, in particular, multiple peaks in the low-temperature specific heat. Due to better treatment of quantum correlations of the intertetramer coupling, an interesting competition between two qualitatively different ground states was uncovered. These ground states are best understood in the limiting cases $J_3 \to 0$ and $J_2 \to 0$. In the limit $J_3 \to 0$ the system is a collection of isolated tetramers, and the ground state for an isolated tetramer is characterized in terms of quantum antiferromagnetic correlations between spins $\mathbf{S}_2$ and $\mathbf{S}_3$ and those between $\mathbf{S}_1$ and $\mathbf{S}_4$. The latter of these relies on the ferromagnetic exchange J_2 as a mediator. On the other hand, in the limit $J_2 \to 0$ the ground state becomes a collection of alternating singlets, one mediated by exchange J_1 and other mediated by J_3. However, this state is accessible only when quantum correlations of the intertetramer interactions are retained. When J_2 and J_3 are both finite, a competition between these qualitatively distinct states is realized. Our study shows that the ground state of the $CuInVO_5$ emerges out of this competition. The above description of the low-temperature magnetism in $CuInVO_5$ is inferred from our analysis of the model for material-specific values of the parameters. We show that an interesting evolution of the competition between different spin-spin correlations exists not only with variation of model parameters but also with increasing temperature. Correlations for certain pairs of spins even increase with increasing temperature, which is contrary to the general expectation that thermal effects reduce the correlations. Magnetic susceptibility calculations further allowed us to identify three distinct regimes in temperature corresponding to a complete paramagnetic behavior at high temperature, a singlet-like behavior at low temperatures, and a mixed

behavior at intermediate temperatures. At intermediate temperatures some of the spins get free from the singlets, while others retain strong singlet correlations. This is consistent with the experimental finding of the magnetization plateau at nearly half the saturation magnetization. By tracking transverse and longitudinal spin-spin correlations, we observe a two-step spin-flop transition in the model. The most important implication of this competition of correlations captured in our CMF study is the existence of multiple peaks in the specific heat, a puzzling feature reported in the experimental data on $CuInVO_5$ [25].

ACKNOWLEDGMENT

We acknowledge the use of the High-Performance Computing Facility at IISER Mohali.

[1] A. Vasiliev, O. Volkova, E. Zvereva, and M. Markina, npj Quantum Mater. **3**, 18 (2018).
[2] T. Giamarchi, in *Understanding Quantum Phase Transitions*, edited by L. D. Carr (Taylor & Francis, London, 2011).
[3] P. Canepa, Y. J. Chabal, and T. Thonhauser, Phys. Rev. B **87**, 094407 (2013).
[4] Y. C. Arango, E. Vavilova, M. Abdel-Hafiez, O. Janson, A. A. Tsirlin, H. Rosner, S.-L. Drechsler, M. Weil, G. Nénert, R. Klingeler, O. Volkova, A. Vasiliev, V. Kataev, and B. Büchner, Phys. Rev. B **84**, 134430 (2011).
[5] A. W. Kinross, M. Fu, T. J. Munsie, H. A. Dabkowska, G. M. Luke, Subir Sachdev, and T. Imai, Phys. Rev. X **4**, 031008 (2014).
[6] A. Oosawa, T. Takamasu, K. Tatani, H. Abe, N. Tsujii, O. Suzuki, H. Tanaka, G. Kido, and K. Kindo, Phys. Rev. B **66**, 104405 (2002).
[7] H. Tanaka, A. Oosawa, T. Kato, H. Uekusa, Y. Ohashi, K. Kakurai, and A. Hoser, J. Phys. Soc. Jpn. **70**, 939 (2001).
[8] T. Nikuni, M. Oshikawa, A. Oosawa, and H. Tanaka, Phys. Rev. Lett. **84**, 5868 (2000).
[9] A. Oosawa, K. Kakurai, T. Osakabe, M. Nakamura, M. Takeda, and H. Tanaka, J. Phys. Soc. Jpn. **73**, 1446 (2004).
[10] A. B. Christian, S. H. Masunaga, A. T. Schye, A. Rebello, J. J. Neumeier, and Y.-K. Yu, Phys. Rev. B **90**, 224423 (2014).
[11] M. G. Banks, F. Heidrich-Meisner, A. Honecker, H. Rakoto, J.-M. Broto, and R. K. Kremer, J. Phys.: Condens. Matter **19**, 145227 (2007).
[12] I. Cabrera, J. D. Thompson, R. Coldea, D. Prabhakaran, R. I. Bewley, T. Guidi, J. A. Rodriguez-Rivera, and C. Stock, Phys. Rev. B **90**, 014418 (2014).
[13] J. Ma, C. D. D. Cruz, T. Hong, W. Tian, A. A. Aczel, S. Chi, J.-Q. Yan, Z. L. Dun, H. D. Zhou, and M. Matsuda, Phys. Rev. B **88**, 144405 (2013).
[14] J. L. Gavilano, E. Felder, D. Rau, H. R. Ott, P. Millet, F. Mila, T. Cichorek, and A. C. Mota, Phys. Rev. B **72**, 064431 (2005).
[15] B. Lake, D. A. Tennant, C. D. Frost, and S. E. Nagler, Nat. Mater. **4**, 329 (2005).
[16] M. B. Stone, D. H. Reich, C. Broholm, K. Lefmann, C. Rischel, C. P. Landee, and M. M. Turnbull, Phys. Rev. Lett. **91**, 037205 (2003).
[17] A. A. Nersesyan and A. M. Tsvelik, Phys. Rev. Lett. **78**, 3939 (1997).
[18] Y. Yoshida, H. Ito, M. Maesato, Y. Shimizu, H. Hayama, T. Hiramatsu, Y. Nakamura, H. Kishida, T. Koretsune, C. Hotta, and G. Saito, Nat. Phys. **11**, 679 (2015).
[19] P. Lecheminant, in *One-Dimensional Quantum Spin Liquids*, edited by H.-T. Diep (World Scientific, Singapore, 2004).
[20] M. Kohno, O. A. Starykh, and L. Balents, Nat. Phys. **3**, 790 (2007).
[21] M. Skoulatos, M. Månsson, C. Fiolka, K. W. Krämer, J. Schefer, J. S. White, and C. Rüegg, Phys. Rev. B **96**, 020414(R) (2017).
[22] Z. Wang, J. Wu, W. Yang, A. K. Bera, D. Kamenskyi, A. T. M. N. Islam, S. Xu, J. M. Law, B. Lake, C. Wu, and A. Loidl, Nature (London) **554**, 219 (2018).
[23] A. K. Bera, B. Lake, F. H. L. Essler, L. Vanderstraeten, C. Hubig, U. Schollwöck, A. T. M. N. Islam, A. Schneidewind, and D. L. Quintero-Castro, Phys. Rev. B **96**, 054423 (2017).
[24] A. Harrison, M. F. Collins, J. Abu-Dayyeh, and C. V. Stager, Phys. Rev. B **43**, 679 (1991).
[25] M. Hase, M. Matsumoto, A. Matsuo, and K. Kindo, Phys. Rev. B **94**, 174421 (2016).
[26] M. Karbach and G. Müller, Phys. Rev. B **62**, 14871 (2000).
[27] H. Kuroe, K. Kusakabe, A. Oosawa, T. Sekine, F. Yamada, H. Tanaka, and M. Matsumoto, Phys. Rev. B **77**, 134420 (2008).
[28] R. Coldea, D. A. Tennant, E. M. Wheeler, E. Wawrzynska, D. Prabhakaran, M. Telling, K. Habicht, P. Smeibidl, and K. Kiefer, Science **327**, 177 (2010).
[29] C. M. Morris, R. Valdés Aguilar, A. Ghosh, S. M. Koohpayeh, J. Krizan, R. J. Cava, O. Tchernyshyov, T. M. McQueen, and N. P. Armitage, Phys. Rev. Lett. **112**, 137403 (2014).
[30] M. Matsuda, S. E. Dissanayake, D. L. Abernathy, K. Totsuka, and A. A. Belik, Phys. Rev. B **92**, 184428 (2015).
[31] M. Hase, A. Matsuo, K. Kindo, and M. Matsumoto, Phys. Rev. B **96**, 214424 (2017).
[32] A. G. Green, G. Conduit, and F. Krüger, Annu. Rev. Condens. Matter Phys. **9**, 59 (2018).
[33] J. D. M. Champion, M. J. Harris, P. C. W. Holdsworth, A. S. Wills, G. Balakrishnan, S. T. Bramwell, E. Čižmár, T. Fennell, J. S. Gardner, J. Lago, D. F. McMorrow, M. Orendáč, A. Orendáčová, D. McK. Paul, R. I. Smith, M. T. F. Telling, and A. Wildes, Phys. Rev. B **68**, 020401(R) (2003).
[34] P. C. Guruciaga, M. Tarzia, M. V. Ferreyra, L. F. Cugliandolo, S. A. Grigera, and R. A. Borzi, Phys. Rev. Lett. **117**, 167203 (2016).
[35] Y.-Z. Ren, N.-H. Tong, and X.-C. Xie, J. Phys.: Condens. Matter **26**, 115601 (2014).
[36] T. Maier, M. Jarrell, T. Pruschke, and M. H. Hettler, Rev. Mod. Phys. **77**, 1027 (2005).
[37] D. Gotfryd, J. Rusnačko, K. Wohlfeld, G. Jackeli, J. Chaloupka, and A. M. Oleś, Phys. Rev. B **95**, 024426 (2017).
[38] N. D. Mermin and H. Wagner, Phys. Rev. Lett. **17**, 1133 (1966).
[39] O. A. Starykh, Rep. Prog. Phys. **78**, 052502 (2015).

[40] E. Dagotto and T. M. Rice, Science **271**, 618 (1996).
[41] C. Balz, B. Lake, H. Luetkens, C. Baines, T. Guidi, M. Abdel-Hafiez, A. U. B. Wolter, B. Büchner, I. V. Morozov, E. B. Deeva, O. S. Volkova, and A. N. Vasiliev, Phys. Rev. B **90**, 060409 (2014).
[42] See Supplemental Material at http://link.aps.org/supplemental/10.1103/PhysRevB.98.104429 for the behavior of C_{23} in Fig. S1.
[43] See Supplemental Material at http://link.aps.org/supplemental/10.1103/PhysRevB.98.104429 for the J_2 dependence of self-consistent mean fields in Fig. S2.
[44] D. C. Johnston, in *Handbook of Magnetic Materials*, edited by K. H. J. Buschow (North-Holland, Amsterdam, 1997), Vol. 10, pp. 1–237.
[45] See Supplemental Material at http://link.aps.org/supplemental/10.1103/PhysRevB.98.104429 for the details of the susceptibility fits.
[46] See Supplemental Material at http://link.aps.org/supplemental/10.1103/PhysRevB.98.104429 for the details of the CMF calculations for the 16-site cluster.
[47] See Supplemental Material at http://link.aps.org/supplemental/10.1103/PhysRevB.98.104429 for results on higher magnetic fields.
[48] D. Yamamoto, Phys. Rev. B **79**, 144427 (2009).
[49] F. M. Zimmer, M. Schmidt, and S. G. Magalhaes, Phys. Rev. E **89**, 062117 (2014).
[50] F. M. Zimmer, M. Schmidt, and J. Maziero, Phys. Rev. E **93**, 062116 (2016).